



Structural design and analysis of a composite wing with high aspect ratio^{*}

Yu-shan MENG, Li YAN^{†‡}, Wei HUANG^{†‡}, Tian-tian ZHANG, Zhao-bo DU

College of Aerospace Science and Engineering, National University of Defense Technology, Changsha, Hunan 410073, China

[†]E-mail: scarlet@163.com; gladrain2001@163.com

Received June 18, 2019; Revision accepted Aug. 21, 2019; Crosschecked Sept. 2, 2019

Abstract: Wings with large aspect ratio have large bending moment and torque, so the poor flexural and torsional stiffness are noteworthy. The application of composite materials in wing structure can improve the performance of wing. In the design process of the wing with high aspect ratio, the design parameters of the wing are preliminarily set. Then, the wing configuration is determined according to the force characteristics referring to the indexes of the Predator unmanned aerial vehicle (UAV), and on the basis of the composite material mechanics and finite element theory, the finite element model of the wing is designed as well. Next, we carry out the aerodynamic analysis in FLUENT. At last, we use ANSYS Composite Pre/Post (ACP) module to establish the static analysis of the wing, and two improvement schemes are proposed to deal with the problem that the wing with high aspect ratio would encounter.

Key words: Composite; High-aspect-ratio wing; Structural design; Finite element static analysis
<https://doi.org/10.1631/jzus.A1900271>

CLC number: V22

1 Introduction

In the phylogeny of aeronautics, the wing plays an important role in the generation of lift force (Sziroczak and Smith, 2016), and its parametric design and optimization have attracted an increasing attention in recent years (Zhang et al., 2016a, 2018; Shen et al., 2019). During the flight, the wing will be over-deformed and even destroyed due to the unstable elastic effects caused by the lack of stiffness (Patil et al., 1998), such as divergence, flutter, and insufficient torsional rigidity, and they have always been prominent factors in reducing flight performance and stability, especially for wings with large aspect ratio. Eskandary et al. (2012) investigated the aeroelastic

properties of a cantilever wing with double bending and torsional vibrations and with large deflection ability in quasi-steady aerodynamics flows, and the influences of mass ratios and stiffness ratios were both taken into consideration. Duan and Zhang (2018) developed a new approach to analyze the aeroelastic stability of a high-aspect-ratio wing based on the transfer function, and it is insensitive to mesh density and does not require structural modal analysis for aeroelastic stability. Farsadi et al. (2018) studied the nonlinear aeroelastic behavior of pretwisted composite high-aspect-ratio wings, and it was structurally modeled as thin walled beams (TWB). Gunasekaran and Mukherjee (2017) implemented a novel de-cambering technique to investigate the influence of wing twist on the induced drag of individual lifting surfaces by means of a vortex lattice approach. As the wingspan increases, the shear force and bending moment caused by the aerodynamic force will increase from the tip to the root. As a result, the tip of the wing will have a larger warpage deformation, and

[‡] Corresponding author

^{*} Project supported by the National Natural Science Foundation of China (No.11972368)

 ORCID: Wei HUANG, <https://orcid.org/0000-0001-9805-985X>

© Zhejiang University and Springer-Verlag GmbH Germany, part of Springer Nature 2019

the wing will be fatigued and broken easily. A nonlinear method based on the computational fluid dynamic and computational structure dynamics (CFD/CSD) coupled approach was employed to analyze the nonlinear static aeroelastic and flutter characteristics of a composite wing with high aspect ratio, and the vertical and spanwise displacements and torsion angle of wing cross-sections are less than the linear result under the same flight attitude (Qiao et al., 2018). Meng et al. (2019) conducted a parametric study on a composite wing with high aspect ratio, and finally an optimal configuration was obtained. However, in their study, the optimization algorithm was not utilized, and this is a useful work for the design of the composite wing with high aspect ratio, as those employed in the design of the transverse injection flow field (Huang, 2014), the thermal protection system (Ou et al., 2019; Sun et al., 2019), the nozzle (Huang et al., 2013a), the cavity flameholder (Huang et al., 2013b; Liao et al., 2018), and the waiver vehicle (Zhang et al., 2016b).

The wing of Predator unmanned aerial vehicle (UAV) is a representative wing with large aspect ratio. The structural design of the wing is more noteworthy considering its long wingspan. However, the strength of the wing cannot increase unlimitedly since the excessive strength will contribute to excessive conservative margin. Instead, it will increase the weight of the structure as well as decrease the performance of the aircraft. Only by combining rigidity with flexibility can we find the perfect midpoint between stiffness and structural performance. Therefore, in this study we designed a wing which is mostly made of carbon fiber composite material and is a large structure with light weight and high rigidity, meanwhile meets the strength requirements of the structure (CAAE, 1990). The application of composite materials enables the wing to produce greater compressive deformation like a shock absorber spring, and this increases the feasibility of bending or deformation of the wing.

Introduced by the above analysis, there is no doubt that the structural design and analysis of the composite wing with high aspect ratio are getting more and more attention. Therefore, in the current study, the composite wing with high aspect ratio has been designed and analyzed by means of the CFD/CSD coupled approach, and two approaches have been developed and employed to improve its per-

formance, namely adding external device to the wing and adding winglets to the wing.

2 Aerodynamic analysis and structural design of wings

The design parameters of the wing are preliminarily formulated according to the indexes of the Predator UAV, as shown in Table 1.

Table 1 Design parameters of the wing

Parameter	Value
Wingspan (m)	14.8
Root chord (m)	1.1
Tip chord (m)	0.4
Cruising Mach number, Ma	0.6
Flight height (m)	7620

The wings designed in this study have a large span, and the flow around the tip of the airfoil will occur. If the wingspan is larger, the flow around the tip is more obvious. A 3D turbulent flow is studied by the computation of the incompressible N-S governing equations, and the finite-volume method is used to discretize the equations. We choose the NACA 2412 airfoil as the physical model for the wing.

In this study, we establish the model in CATIA and transmit it into ANSYS to generate structural grid. Then, the aerodynamic analysis of NACA 2412 is carried out by the commercial software FLUENT. In this process, the flight parameters are imported, and the operating conditions are set. At the same time, the monitor is defined. After initializing the flow field, 3000 iteration steps are set up, and the CFD POST post-processing software is started to process the data after the iteration curve converges. The lift and drag characteristics are remarkable. After the calculation is completed, the lift-drag ratio is obtained as 30.2, which meets the requirements of high lift-drag ratio of the wing.

In the modeling process, we simplify the wing into a structure with skin, beams, and ribs. It adopts a double-beam structure with high bearing efficiency (Zhang et al., 2005). The size of the beam will not be particularly large considering that the skin of the wing can provide part of the flexural stiffness. The widths of the upper and lower flanges of the fore-beam are

both 110 mm, and the thickness is 10 mm. The rear beam acts as an auxiliary beam, and the widths of the upper and lower flanges are 80 mm with the thickness being 10 mm. The thickness of the web is 10 mm as well. According to the characteristics of NACA 2412 airfoil and the bearing requirements of the structure, the front beam is placed at 29% away from the leading edge and the rear beam is set at 58% away from the leading edge.

So as to facilitate the research of this paper, we simplify the ribs into a web structure. The most appropriate distance between two adjacent ribs is from 500 mm to 600 mm, which has been found to be the optimum (Zhao, 2016). Here, we set the distance to 560 mm. Fourteen identical wing ribs are used; at the root of the wing is a reinforced wing rib, and the rest are normal wing ribs. Without changing stress distribution, holes are set on the wing ribs in order to decrease weight. According to the size parameters proposed above, Fig. 1 presents the model of the internal structure of the wing.

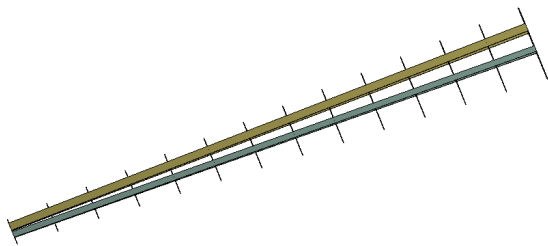


Fig. 1 Internal structure of the wing

3 Finite element static analysis of composite wings

In this study, we establish a finite element analysis based on ANSYS Composite Pre/Post (ACP) module. The ANSYS ACP composite material special module is the pre- and post-processing module of the composite material analysis scheme (Li et al., 2017). The ANSYS ACP module uses the micro-analysis approach to carry out the finite element modeling and material analysis. The structure can simulate the actual structure of the shell accurately, realize data transmission with other modules of ANSYS, and realize the design, manufacture, and functional verification of composite products through the combina-

tion with the solver. The ACP module contains two sub-modules, namely pre-processing and post-processing. In the pre-processing module, the properties of the material adopted in the structure which include material density are created, and boundary conditions are set. In the post-processing module, the resolving result file is imported into the process to evaluate and visualize the composite structure. The pre- and post-processing workflow is shown in Fig. 2.



Fig. 2 Pre- and post-processing workflow for finite element modeling and material analysis

The simulation basis of the ACP composite modeling module is the shell unit. The difference between the basic workflow of shell element and that of solid element is that when transferring data, the shell element needs to select the transfer shell composite data option to transfer the data of shell element to the static analysis module, which is actually the equivalent stiffness of multi-layer material. For composite shell element, the anisotropic laminated plate theory is used, and the finite element analysis is more complicated than the isotropic metal shell. When analyzing composite shell elements, we use the theory of anisotropic laminate thin shells, which is more complicated than the isotropic metal shell structure in the finite element analysis.

In order to deal with the poor shear resistance of composite material, the beam structure adopts aluminum alloy material while the composite material is used for skin and wing ribs. The material parameters are shown in Tables 2 and 3.

Table 2 Properties of aluminum alloy

Parameter	Value
Density, ρ (kg/m ³)	2780
Elastic Modulus, E (GPa)	70 610
Poisson's ratio, μ	0.3
Tensile ultimate strength, σ_b (MPa)	432

As for wing ribs, they are used as structures to withstand shear forces, so $\pm 45^\circ$ are used entirely (Editorial Committee of Aircraft Design Handbook, 2000). The thickness of reinforced wing rib is 9 mm, which has nine layer groups. Meanwhile, the thickness of normal wing rib is 6 mm, which has four layer groups. Ten layers are designed in each group, the single thickness of which is 0.15 mm.

Table 3 Properties of epoxy matrix composite

Parameter	Value
Density, ρ (kg/m ³)	1600
Elastic modulus in x direction, E_1 (GPa)	181
Elastic modulus in y direction, E_2 (GPa)	10.3
Poisson's ratio in xy directions, μ_{12}	0.28
Shear modulus in xy directions, G_{12} (GPa)	7.17
Tensile in x direction, X (MPa)	1500
Compressive in x direction, X' (MPa)	1500
Tensile in y direction, Y (MPa)	40
Compressive in y direction, Y' (MPa)	246
Shear, S (MPa)	68

The ability of the wing to resist deformation and failure depends largely on the performance of the skin, the deformation of the wing can be controlled by controlling the tension of the skin. Meanwhile, in the process of finite element analysis, the influence of the thickness of the skin is taken into account. Since the skin is expected to have excellent structure strength and bending resistance to withstand aerodynamic loads and bending moments, it is required that the skin of the wing has appropriate thickness. Therefore, in order to ensure that the wing can maintain the highest areodetic efficiency during flying and choose the most appropriate thickness of the skin, the research of six groups with different thicknesses is carried out separately. Taking the skin thickness as the design variable, the maximum deformation and failure coefficient of the wing are analyzed and compared by using the obtained aerodynamic load. On account of weight and rigidity, the effectiveness of each layer is taken as the standard in this study.

The parameters of skin layers with different thicknesses are shown in Table 4.

To conduct a comprehensive study, a comparison of skins with different thicknesses is carried out in ACP module.

1. When the thickness of skin is 4 mm, the maximum deformation of the wing is 1031.5 mm, the maximum stress of the upper wing is 713.55 MPa, and the maximum layer stress of the lower wing is 734.76 MPa, as shown in Figs. 3–5.

Table 4 Skin layer parameters of different thicknesses

Thickness (mm)	Number of layer groups	Layers of each group	Thickness of single layer (mm)
4	4	10	0.100
6	4	10	0.150
8	5	10	0.160
10	8	10	0.125
12	10	10	0.120
14	7	10	0.200

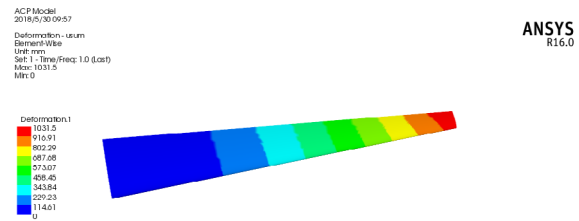


Fig. 3 Deformation cloud diagram (skin thickness is 4 mm)

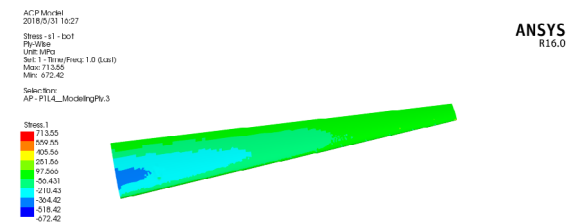


Fig. 4 Stress cloud diagram of upper wing (skin thickness is 4 mm)

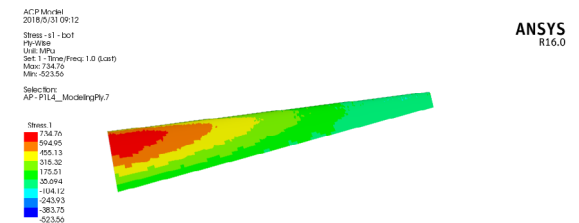


Fig. 5 Stress cloud diagram of lower wing (skin thickness is 4 mm)

2. When the thickness of skin is 6 mm, the maximum deformation of the wing is 873.67 mm, the maximum stress of the upper wing is 605.94 MPa, and the maximum layer stress of the lower wing is 604.69 MPa (Figs. 6–8).

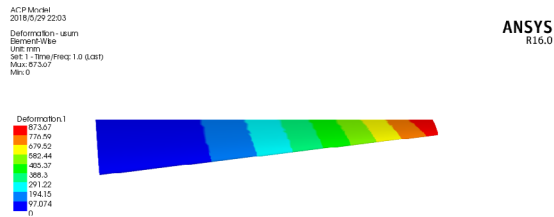


Fig. 6 Deformation cloud diagram (skin thickness is 6 mm)

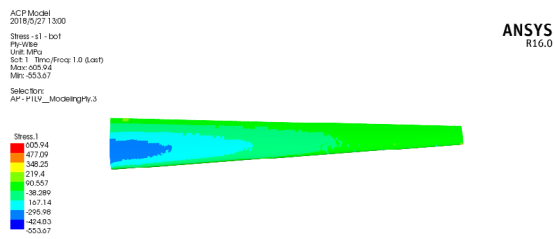


Fig. 7 Pressure cloud diagram of upper wing (skin thickness is 6 mm)

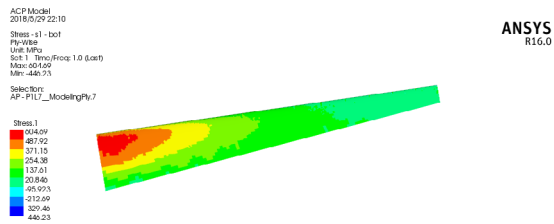


Fig. 8 Pressure cloud diagram of lower wing (skin thickness is 6 mm)

3. When the thickness of skin is 8 mm, the deformation cloud diagram and stress cloud diagram are obtained as shown in Figs. 9–11.

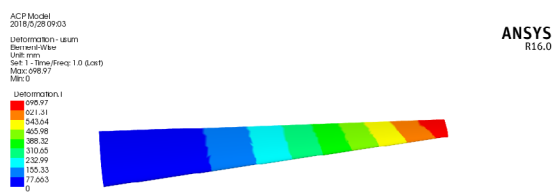


Fig. 9 Deformation cloud diagram (skin thickness is 8 mm)

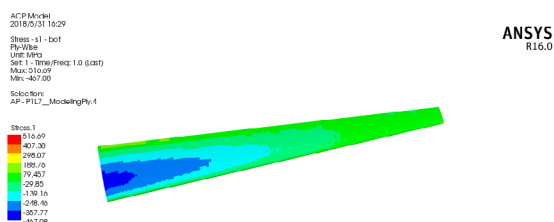


Fig. 10 Stress cloud diagram of upper wing (skin thickness is 8 mm)

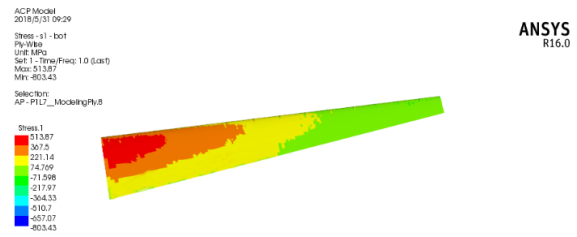


Fig. 11 Stress cloud diagram of lower wing (skin thickness is 8 mm)

It can be seen from the stress cloud diagrams above that when the skin thickness is 4 mm, 6 mm, and 8 mm, respectively, the failure coefficient of each layer is much larger than 1. The stress and the failure coefficient are the largest at the junction of the wing root and the flange of the front beam. This is because the aerodynamic force of the wing near the leading edge is the largest, and the front beam of the wing bears the most of bending moments. It is no longer an effective way to purely increase the thickness of the skin, while it is feasible to increase the size of the front beam from 10 mm to 12 mm, and the thickness of the upper and lower flanges should be increased from 8 mm to 10 mm. Then, the thickness of the skin is further increased until the skin meets the strength requirements of the wing.

4. After changing the size of the beam, when the thickness of skin is 10 mm, the maximum deformation of the wing decreases and the strength increases at a certain level, but the failure coefficient is still greater than 1 (Figs. 12–14). Hence, the skin thickness is expected to be further increased.

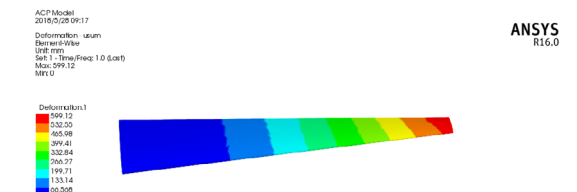


Fig. 12 Deformation cloud diagram (skin thickness is 10 mm)

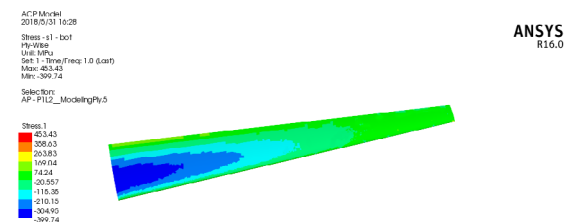


Fig. 13 Stress cloud diagram of upper wing (skin thickness is 10 mm)

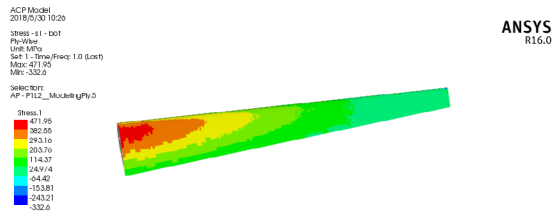


Fig. 14 Stress cloud diagram of lower wing (skin thickness is 10 mm)

When the thickness of skin is increased to 12 mm, the maximum deformation of the wing is 420.56 mm, the maximum stress of the upper wing is 365.37 MPa, and the maximum layer stress of the lower wing is 363.24 MPa. When the thickness of skin is 14 mm, the deformation cloud diagram and stress cloud diagram are obtained as shown in Figs. 15–17.

Figs. 15–17 depict that when the thickness of skin is 14 mm, the maximum deformation is 322.25 mm, the maximum stress of the upper wing is 320.02 MPa, and the maximum stress of the lower wing is 321.23 MPa. The mechanical properties of different skin thicknesses are listed in Table 5.

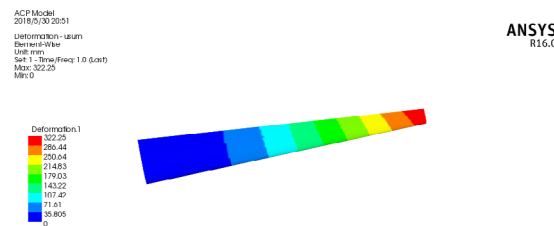


Fig. 15 Deformation cloud diagram (skin thickness is 14 mm)

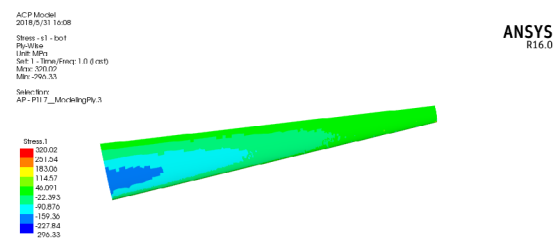


Fig. 16 Stress cloud diagram of upper wing (skin thickness is 14 mm)

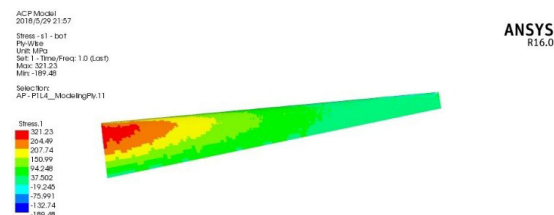


Fig. 17 Stress cloud diagram of lower wing (skin thickness is 14 mm)

Table 5 Mechanical properties of different skin thicknesses

Thickness (mm)	Maximum deformation (mm)	Maximum stress of upper wing (MPa)	Maximum failure coefficient of wing
4	1031.5	713.55	4.0353
6	873.67	605.94	3.1540
8	698.17	516.69	1.9430
10	599.12	453.43	0.95074
12	420.56	365.37	0.61564
14	322.25	320.02	0.49358

As shown in Table 5, when the thickness of the skin is up to 12 mm, it has already met the strength requirements of the wing, and the failure coefficient of each layer is much smaller than 1. Considering synthetically the weight and strength of the structure, 12 mm is selected as the proper thickness of the skin in this study.

4 Optimization and improvement of composite wings with high aspect ratio

According to the analysis above, the deformation of the wing is relatively large. However, due to the current requirements of the composite material for the manufacturing process and the limitations of manufacturing costs, the application of composite wing structures has not been particularly extensive. Therefore, if the bending deformation of the wing need to be further reduced, some optimal improvement design should be conducted.

Two methods are used to improve the performance of the wing. The first method is to add external device to the wing in order to offset the upward momentum, and use the weight of the external device to offset a part of the lift of the wing so as to reduce the bending deformation trend of the wing. The second method is to add winglets to the wing tip in order to increase the effective span of the wing, thus improving the large bending deformation of the wing with high aspect ratio indirectly.

4.1 Adding external device to the wing

The position of external device is usually determined by the pressure center of the wing, and it is usually placed at the front of the pressure center of the wing. After simulation in the commercial software FLUENT, the approximate position of the pressure

center of the wing is 3.12 m away from the root of the wing.

In the current study, the external device is regarded as a line load. Open the static analysis module, and load line pressure of 37.69 N/mm uniformly on the line with the length of 380 mm between the wing ribs. The whole process is shown in Fig. 18.

The location of the plug-in is varied separately. In order to show the location of the external service more intuitively, planar graphs as cases 1–4 are shown in Fig. 19. After applying the load, when the center of gravity of the external device is 20% behind the gravity line, the maximum deformation of the

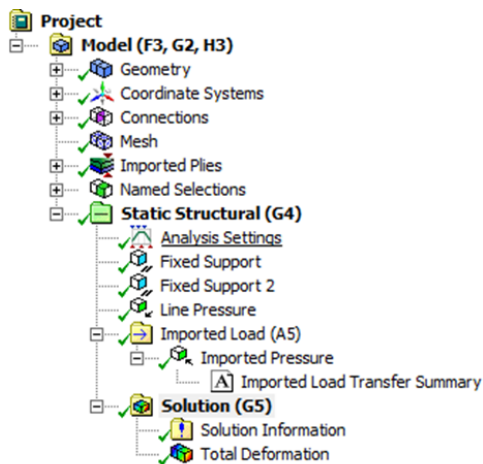


Fig. 18 Whole process of the static analysis

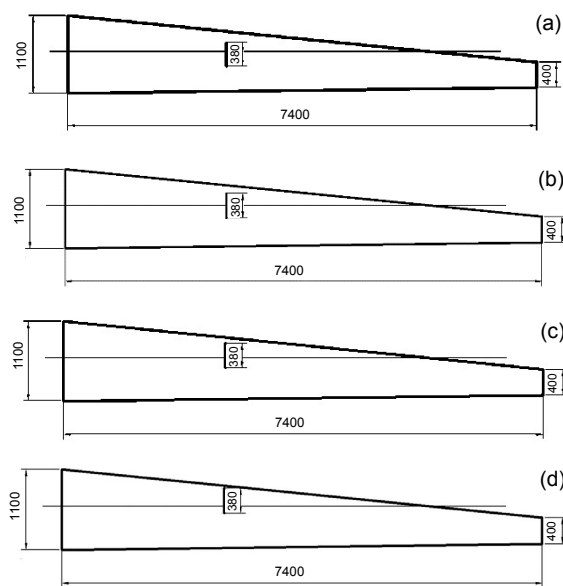


Fig. 19 Planar graphs for different cases (a) Case 1; (b) Case 2; (c) Case 3; (d) Case 4

wing is 322.25 mm, the maximum stress of the upper wing is 320.02 MPa, and the maximum layer stress of the lower wing is 321.23 MPa (Figs. 20–22).

After applying the load, when the center of gravity of the external device is exactly on the gravity line, the maximum deformation of the wing is 279.32 mm, the maximum stress of the upper wing is 317.35 MPa, and the maximum layer stress of the lower wing is 313.41 MPa (Figs. 23–25).

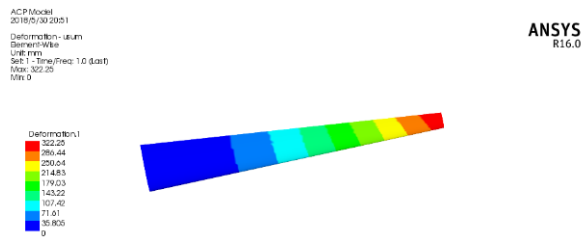


Fig. 20 Deformation cloud diagram when the center of gravity of the external device is 20% behind the gravity line

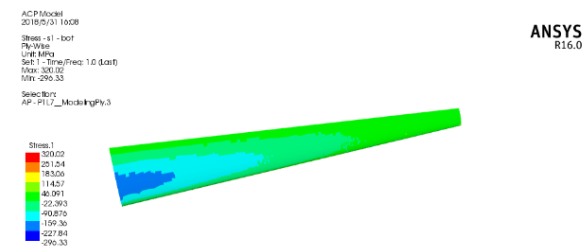


Fig. 21 Stress cloud diagram of the upper wing when the center of gravity of the external device is 20% behind the gravity line

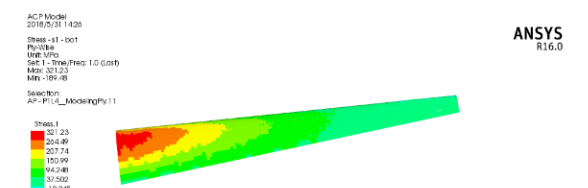


Fig. 22 Stress cloud diagram of the lower wing when the center of gravity of the external device is 20% behind the gravity line

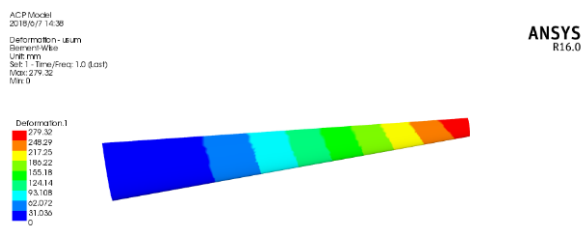


Fig. 23 Deformation cloud diagram when the center of gravity of the external device is exactly on the gravity line

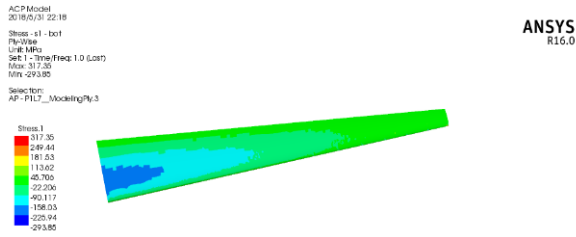


Fig. 24 Stress cloud diagram of the upper wing when the center of gravity of the external device is exactly on the gravity line

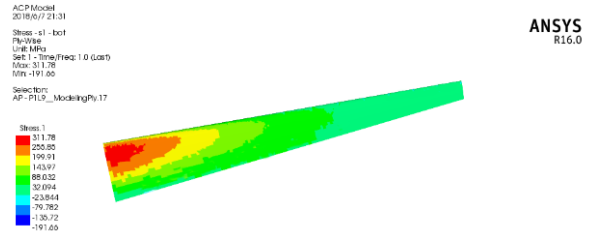


Fig. 28 Cloud diagram of the lower wing when the center of gravity of the external device is 15% before the gravity line

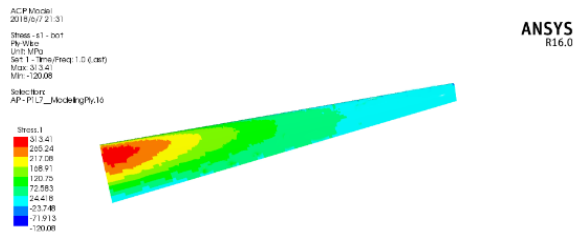


Fig. 25 Stress cloud diagram of the lower wing when the center of gravity of the external device is exactly on the gravity line

After applying the load, when the center of gravity of the external device is 25% before the gravity line, the maximum deformation of the wing is 247.58 mm, the maximum stress of the upper wing is 302.97 MPa, and the maximum layer stress of the lower wing is 310.43 MPa (Figs. 29–31).

After applying the load, when the center of gravity of the external device is 15% before the gravity line, the maximum deformation of the wing is 216.14 mm, the maximum stress of the upper wing is 309.34 MPa, and the maximum layer stress of the lower wing is 311.78 MPa (Figs. 26–28).

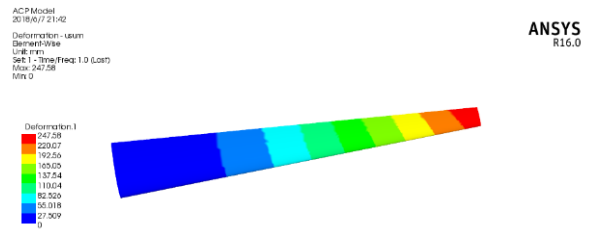


Fig. 29 Deformation cloud diagram when the center of gravity of the external device is 25% before the gravity line

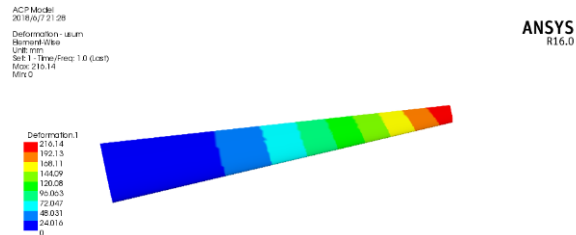


Fig. 26 Deformation cloud diagram when the center of gravity of the external device is 15% before the gravity line

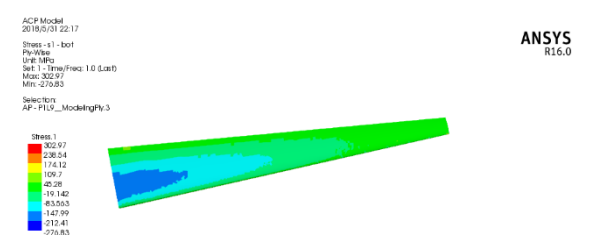


Fig. 30 Stress cloud diagram of the upper wing when the center of gravity of the external device is 25% before the gravity line

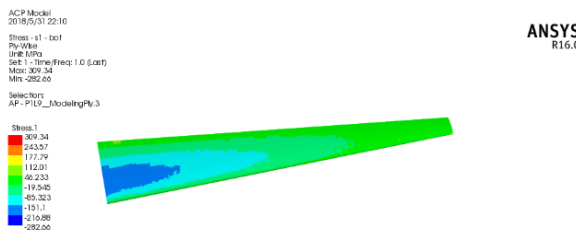


Fig. 27 Stress cloud diagram of the upper wing when the center of gravity of the external device is 15% before the gravity line

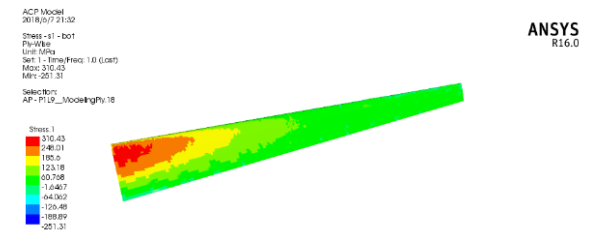


Fig. 31 Stress cloud diagram of the lower wing when the center of gravity of the external device is 25% before the gravity line

When the center of gravity of the external device is at different positions of the gravity line, it can be seen from the difference ratio in Table 6 that the lift moment is partly offset by the weight of the external device itself. When the external device is at different positions, the maximum deformation of the wingtip decreases compared with the condition that there is no external device, and the maximum stresses of the upper and lower wing surfaces decrease. Especially, when the center of gravity of the external device is 15% before the gravity line, the deformation of the tip is the smallest, and the maximum deformation of the wing is 216.14 mm, which is 204.42 mm less than the initial deformation of the structure.

When the center of gravity of the external device is behind the center of gravity line, the maximum deformation of the wing is 322.25 mm, which is the largest compared with the other positions. Therefore, when the load is applied and the wing is subjected to large deformation, the unfavorable deformation can be reduced by adding external device at 15% before the gravity line.

Table 6 Deformation comparison for cases with external device at difference positions

Position	Maximum deformation (mm)	Initial deformation (mm)	Unbalance rate (%)
20% behind the gravity line	322.25	420.56	23.38
On the gravity line	279.32	420.56	33.58
15% before the gravity line	216.14	420.56	48.61
25% before the gravity line	247.58	420.56	41.13

4.2 Add winglets to the wing

In addition to reducing the deformation of the wings by adding external device to the wings mentioned above, the performance of the wings can also be improved by changing the shape of the wing. The Boeing 787 adopts upward curved wings with carbon fiber structure to improve the performance of the aircraft.

In this part, the winglet is adopted as the improvement device to improve the efficiency of the

wing, and this is the same as that employed in the vertical axis wind turbine (Zhang et al., 2019). This method not only increases the wingspan of the wing to a certain extent, but also reduces the airflow flowing from the lower surface of the wing to the upper surface and increases the lift-to-drag ratio. Fig. 32 shows the shape of the wing after adding winglets with a height of 400 mm.

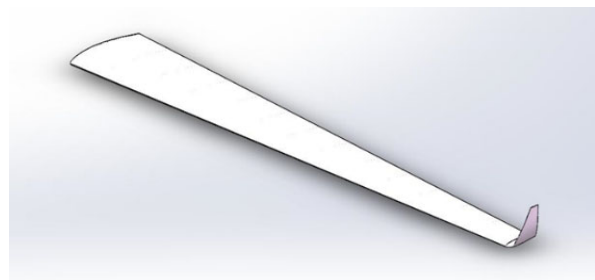


Fig. 32 Shape of the wing with a winglet

Under the same load, the height of the winglet is varied to compare the performance of the wing. When the height of the winglet is 150 mm, the deformation cloud diagram and stress cloud diagrams are obtained as Figs. 33–35.

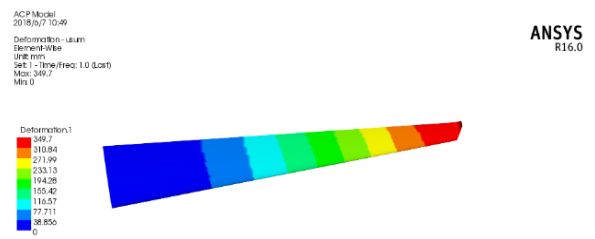


Fig. 33 Deformation cloud diagram when the height of the winglet is 150 mm

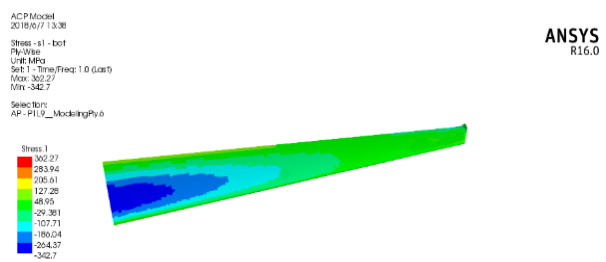


Fig. 34 Stress cloud diagram of the upper wing when the height of the winglet is 150 mm

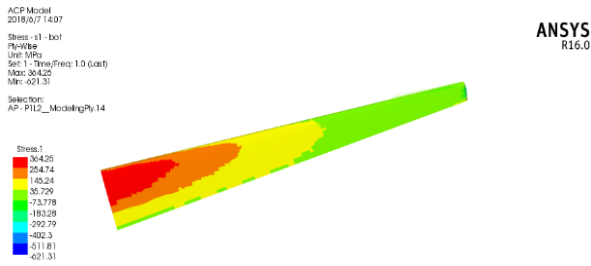


Fig. 35 Stress cloud diagram of the lower wing when the height of the winglet is 150 mm

In the following cases, the stresses on the upper and lower wing surfaces are of the same order, and they are all about 460 MPa. The maximum deformations with different heights of the winglet are compared below.

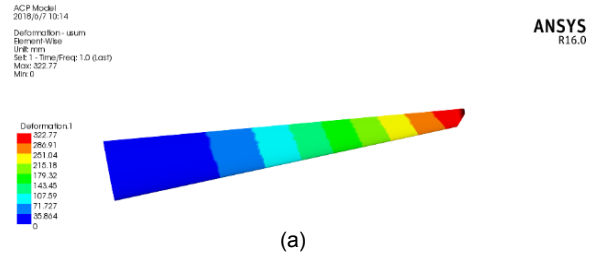
When the height of the winglet changes from 200 mm to 400 mm, the deformation cloud diagrams are obtained as Figs. 36a–36e.

The analysis results of wings with different heights of the winglet are listed in Table 7.

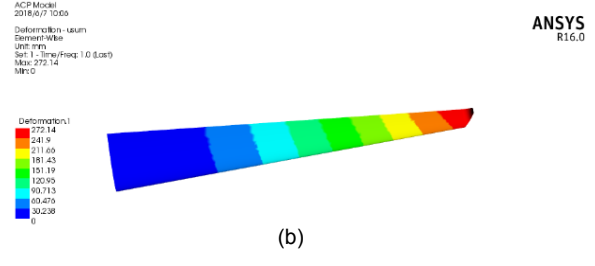
Table 7 Deformation comparison for cases with different heights of the winglet

Winglet height (mm)	Maximum deformation (mm)	Initial deformation (mm)	Unbalance rate (%)
150	349.70	420.56	16.85
200	322.22	420.56	23.25
250	272.77	420.56	35.14
300	222.78	420.56	47.02
350	279.04	420.56	33.65
400	336.81	420.56	19.91

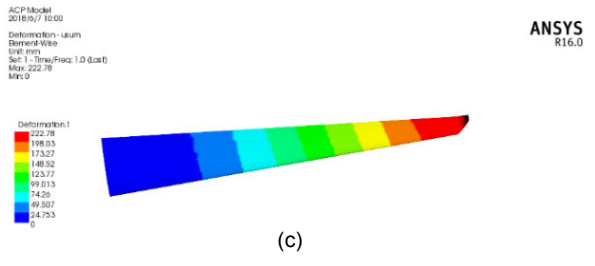
From the data in Table 7, it can be seen that the maximum deformation of the tip of the wing decreases when the winglet is added to the wingtip, but the height of the winglet is not the higher the better. When the height of the winglet is 300 mm, the maximum deformation of the wing decreases the most, and this is 197.78 mm less than the original one (i.e. a reduction of almost 47.03%). Therefore, it is concluded that for the composite wing designed in this study, the maximum deformation of the wing can be reduced the most by adding the winglet with a height of 300 mm to the wing.



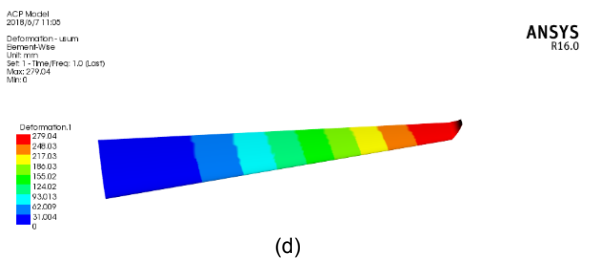
(a)



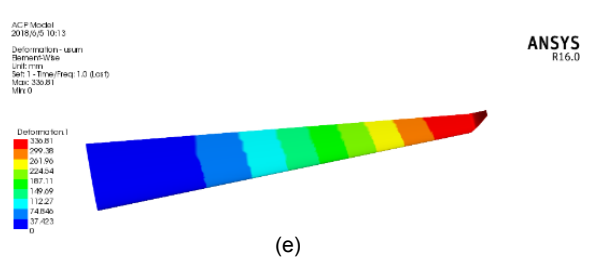
(b)



(c)



(d)



(e)

Fig. 36 Deformation cloud diagrams for cases with different heights of the winglet: (a) 200 mm; (b) 250 mm; (c) 300 mm; (d) 350 mm; (e) 400 mm

5 Comparison of wings made of different materials

Before the composite materials became widespread, aluminum alloy was the most commonly used

material in aerospace field. Hence, for the purpose of confirming that composite wing has the features of higher strength and lighter weight, a comparison of wings made of different materials is carried out. The mass of full-metal wing is 382.41 kg, while the mass of full-composite wing is 220.09 kg, which is 42.45% lower than that of the full-metal wing. It is clear that the composite has excellent weight reduction effect. As for the full-composite wing, the layup design of beam structure is also discussed here. The front beam and the back beam are also separately layered, and 45° is adopted as the ply angle of webs to bear the shearing force. The layup method of upper and lower flanges is designed as $[45/90/0/90/-45]_s$ symmetrically. Table 8 depicts the comparisons of wings made of different materials. Compared with the full-metal wing, the mechanical properties of the full-composite wing are excellent. In the same conditions, the maximum deformation of the full-composite wing reduces 44.83% compared with the full-metal model, which proves that the full-composite material is the most effective.

Table 8 Structural performance of different materials

Material	Maximum stress (MPa)	Maximum deformation (mm)
Semi-composite wing	344.35	380.39
Full-composite wing	309.34	315.00
Full-metal wing	263.88	570.97
Unbalance rate (full-composite wing with full-metal wing)	17.20%	44.83%

6 Conclusions

In this paper, we use ANSYS to establish finite element models to study the performance of a composite wing with large aspect ratio. Firstly, the aerodynamic shape of the wing is designed, and the structure type and component dimensions are proposed initially. Then, the ACP module of ANSYS Workbench is adopted to perform the stress analysis, which includes the material setup, large deformation, and contact condition. Finally, in view of the inevitable structural deformation problem of the wing in process of flight, considering the cost limitation and

feasibility of manufacturing process, two improvement schemes are proposed at the end of this paper. There are some meaningful observations in this study which are presented as follows:

1. After calculating and comparing the structural properties of skins with different thicknesses, the most suitable thickness of the skin is obtained as 12 mm, which meets the requirements of weight and strength.

2. The first design scheme is to add external device to the wing in order to offset the upward momentum, and use the weight of the external device to offset a part of the lift of the wing so as to reduce the bending deformation trend of the wing. Especially, when the center of gravity of the external device is 15% before the gravity line, the deformation of the tip is the smallest, and this is 204.42 mm less than the initial deformation of the structure.

3. The second design scheme is to add winglet at the tip of the wing to increase the effective span of the wing, thus improving the large bending deformation of the wing indirectly. When the height of the winglet is 300 mm, the maximum deformation of the wing reduces almost 47.03% compared with that of the base model.

4. It is very significant to use composite materials in wings with high aspect ratio. Under the same analytical conditions, the deformation of the full-composite wing is smaller than that of full-metal wing. Meanwhile, the total weight of the full-composite wing reduces almost 42.45% compared with that of the full-metal wing.

Contributors

Yu-shan MENG designed the research and wrote the first draft of the manuscript. Tian-tian ZHANG and Zhao-bo DU helped organize the manuscript. Li YAN and Wei HUANG revised and edited the final version.

Conflict of interest

Yu-shan MENG, Li YAN, Wei HUANG, Tian-tian ZHANG, and Zhao-bo DU declare that they have no conflict of interest.

References

- CAAE (Chinese Aeronautics and Astronautics Establishment), 1990. Composite Material Structure Design Manual. Aviation Industry Press, Beijing, China (in Chinese).

- Duan JB, Zhang ZY, 2018. Aeroelastic stability analysis of aircraft wings with high aspect ratios by transfer function method. *International Journal of Structural Stability and Dynamics*, 18(12):1850150.
<https://doi.org/10.1142/S021945541850150X>
- Editorial Committee of Aircraft Design Handbook, 2000. Air-plane Design Handbook: Book 10. Aviation Industry Press, Beijing, China (in Chinese).
- Eskandary K, Dardel M, Pashaei MH, et al., 2012. Nonlinear aeroelastic analysis of high-aspect-ratio wings in low subsonic flow. *Acta Astronautica*, 70:6-22.
<https://doi.org/10.1016/j.actaastro.2011.07.017>
- Farsadi T, Rahmanian M, Kayran A, 2018. Geometrically nonlinear aeroelastic behavior of pretwisted composite wings modeled as thin walled beams. *Journal of Fluids and Structures*, 83:259-292.
<https://doi.org/10.1016/j.jfluidstructs.2018.08.013>
- Gunasekaran M, Mukherjee R, 2017. Behaviour of trailing wing(s) in echelon formation due to wing twist and aspect ratio. *Aerospace Science and Technology*, 63:294-303.
<https://doi.org/10.1016/j.ast.2017.01.009>
- Huang W, 2014. Design exploration of three-dimensional transverse jet in a supersonic crossflow based on data mining and multi-objective design optimization approaches. *International Journal of Hydrogen Energy*, 39(8):3914-3925.
<https://doi.org/10.1016/j.ijhydene.2013.12.129>
- Huang W, Wang ZG, Ingham DB, et al., 2013a. Design exploration for a single expansion ramp nozzle (SERN) using data mining. *Acta Astronautica*, 83:10-17.
<https://doi.org/10.1016/j.actaastro.2012.09.016>
- Huang W, Liu J, Yan L, et al., 2013b. Multiobjective design optimization of the performance for the cavity flameholder in supersonic flows. *Aerospace Science and Technology*, 30(1):246-254.
<https://doi.org/10.1016/j.ast.2013.08.009>
- Li ZY, Kan C, Zhang CC, 2017. Finite Element Analysis and Application of Composite Materials Based on ANSYS. China Water & Power Press, Beijing, China, p.32-34 (in Chinese).
- Liao L, Yan L, Huang W, et al., 2018. Mode transition process in a typical strut-based scramjet combustor based on a parametric study. *Journal of Zhejiang University-SCIENCE A (Applied Physics & Engineering)*, 19(6):431-451.
<https://doi.org/10.1631/jzus.A1700617>
- Meng YS, Yan L, Huang W, et al., 2019. Detailed parametric investigation and optimization of a composite wing with high aspect ratio. *International Journal of Aerospace Engineering*, 2019:3684015.
<https://doi.org/10.1155/2019/3684015>
- Ou M, Yan L, Huang W, et al., 2019. Design exploration of combinational spike and opposing jet concept in hypersonic flows based on CFD calculation and surrogate model. *Acta Astronautica*, 155:287-301.
<https://doi.org/10.1016/j.actaastro.2018.12.012>
- Patil MJ, Hodges DH, Cesnik CES, 1998. Nonlinear aeroelastic analysis of aircraft with high-aspect-ratio wings. Proceedings of the 39th AIAA/ASME/ASCE/AHS/ASC Structures, Structural Dynamics, and Materials Conference and Exhibit.
<https://doi.org/10.2514/6.1998-1955>
- Qiao SJ, Gao HS, Lyu Y, et al., 2018. Nonlinear aeroelastic characteristics analysis of composite wing with high aspect ratio based on co-rotational method. *Journal of Fluids and Structures*, 82:619-637.
<https://doi.org/10.1016/j.jfluidstructs.2018.07.009>
- Shen Y, Huang W, Zhang TT, et al., 2019. Parametric modeling and aerodynamic optimization of EXPERT configuration at hypersonic speeds. *Aerospace Science and Technology*, 84:641-649.
<https://doi.org/10.1016/j.ast.2018.11.007>
- Sun XW, Huang W, Ou M, et al., 2019. A survey on numerical simulations of drag and heat reduction mechanism in supersonic/hypersonic flows. *Chinese Journal of Aeronautics*, 32(4):771-784.
<https://doi.org/10.1016/j.cja.2018.12.024>
- Sziroczak D, Smith H, 2016. A review of design issues specific to hypersonic flight vehicles. *Progress in Aerospace Sciences*, 84:1-28.
<https://doi.org/10.1016/j.paerosci.2016.04.001>
- Zhang JK, Li ZN, Kou CH, 2005. Structural design of high aspect ratio composite material wing. *Acta Aeronautica Et Astronautica Sinica*, 26(4):450-453.
- Zhang TT, Wang ZG, Huang W, et al., 2016a. Parameterization and optimization of hypersonic-gliding vehicle configurations during conceptual design. *Aerospace Science and Technology*, 58:225-234.
<https://doi.org/10.1016/j.ast.2016.08.020>
- Zhang TT, Huang W, Wang ZG, et al., 2016b. A study of airfoil parameterization, modeling, and optimization based on the computational fluid dynamics method. *Journal of Zhejiang University-SCIENCE A (Applied Physics & Engineering)*, 17(8):632-645.
<https://doi.org/10.1631/jzus.A1500308>
- Zhang TT, Wang ZG, Huang W, et al., 2018. A review of parametric approaches specific to aerodynamic design process. *Acta Astronautica*, 145:319-331.
<https://doi.org/10.1016/j.actaastro.2018.02.011>
- Zhang TT, Elsakka M, Huang W, et al., 2019. Winglet design for vertical axis wind turbines based on a design of experiment and CFD approach. *Energy Conversion and Management*, 195:712-726.
<https://doi.org/10.1016/j.enconman.2019.05.055>
- Zhao AY, 2016. The layout of ribs in the wingbox for modern civil aircraft. *Science & Technology Vision*, (14):115 (in Chinese).
<https://doi.org/10.19694/j.cnki.issn2095-2457.2016.14.077>

中文概要

题目: 大展弦比复合材料机翼结构设计与分析

目的: 大展弦比机翼具有弯矩较大、扭转刚度较差的特点。在机翼结构上利用复合材料能很好地改善机翼结构性能。本文旨在设计一个满足刚度和强度要求的大展弦比复合材料机翼, 并对大展弦比机翼遇到的大变形问题提出改进方案。

创新点: 1. 通过流固耦合的方法对大展弦比机翼进行气动仿真和有限元静力分析; 2. 针对大展弦比机翼产生的大变形现象, 提出增加机翼外挂或在翼尖处增加翼尖小翼的方法进行改进。

方法: 1. 通过数值仿真建立机翼的有限元模型, 并对机翼进行气动分析; 2. 通过流固耦合, 将在 FLUENT

中的气动力加载到有限元静力分析模块进行分析; 3. 通过 Workbench 中的 ACP 复合材料专用模块, 对复合材料结构进行铺层。

结论: 1. 综合考虑刚度、强度以及减重效果, 确定 12 mm 为本文大展弦比复合材料机翼的最佳蒙皮厚度; 2. 利用增加外挂的方法减小机翼大变形时, 当外挂重心位置在机翼重心线前 15% 时机翼变形减小的程度最大; 3. 在翼尖处增加高度为 300 mm 的翼尖小翼时机翼变形减小程度最大。4. 在相同受载情况下, 相比于金属材料机翼, 复合材料机翼结构能够有效减小机翼的翼尖最大位移和最大应力。

关键词: 复合材料; 大展弦比机翼; 结构设计; 有限元静力分析